

Plume Measurements with the T5 Xenon Ion Thruster

30 September 1994

Prepared by

J. E. POLLARD
Mechanics and Materials Technology Center
Technology Operations

Prepared for

SPACE AND MISSILE SYSTEMS CENTER
AIR FORCE MATERIEL COMMAND
2430 E. El Segundo Boulevard
Los Angeles Air Force Base, CA 90245

Development Group

19941205 058

APPROVED FOR PUBLIC RELEASE;
DISTRIBUTION UNLIMITED

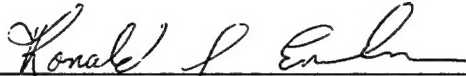


**THE AEROSPACE
CORPORATION**
El Segundo, California

This report was submitted by The Aerospace Corporation, El Segundo, CA 90245-4691, under Contract No. F04701-93-C-0094 with the Space and Missile Systems Center, 2430 E. El Segundo Blvd., Los Angeles Air Force Base, CA 90245. It was reviewed and approved for The Aerospace Corporation by S. Feuerstein, Principal Director, Mechanics and Materials Technology Center.

This report has been reviewed by the Public Affairs Office (PAS) and is releasable to the National Technical Information Service (NTIS). At NTIS, it will be available to the general public, including foreign nationals.

This technical report has been reviewed and is approved for publication. Publication of this report does not constitute Air Force approval of the report's findings or conclusions. It is published only for the exchange and stimulation of ideas.

A handwritten signature in cursive script, reading "Ronald S. Einhorn", is written over a horizontal line.

Ronald S. Einhorn, Captain, USAF
SMC/XRI

REPORT DOCUMENTATION PAGE

Form Approved
OMB No. 0704-0188

Public reporting burden for this collection of information is estimated to average 1 hour per response, including the time for reviewing instructions, searching existing data sources, gathering and maintaining the data needed, and completing and reviewing the collection of information. Send comments regarding this burden estimate or any other aspect of this collection of information, including suggestions for reducing this burden to Washington Headquarters Services, Directorate for Information Operations and Reports, 1215 Jefferson Davis Highway, Suite 1204, Arlington, VA 22202-4302, and to the Office of Management and Budget, Paperwork Reduction Project (0704-0188), Washington, DC 20503.

1. AGENCY USE ONLY (Leave blank)		2. REPORT DATE 30 September 1994		3. REPORT TYPE AND DATES COVERED	
4. TITLE AND SUBTITLE Plume Measurements with the T5 Xenon Ion Thruster				5. FUNDING NUMBERS F04701-93-C-0094	
6. AUTHOR(S) Pollard, James E.					
7. PERFORMING ORGANIZATION NAME(S) AND ADDRESS(ES) The Aerospace Corporation Technology Operations El Segundo, CA 90245-4691				8. PERFORMING ORGANIZATION REPORT NUMBER TR-94(4507)-2	
9. SPONSORING/MONITORING AGENCY NAME(S) AND ADDRESS(ES) Space and Missile Systems Center Air Force Materiel Command 2340 E. El Segundo Boulevard Los Angeles Air Force Base, CA 90245				10. SPONSORING/MONITORING AGENCY REPORT NUMBER SMC-TR-94-44	
11. SUPPLEMENTARY NOTES					
12a. DISTRIBUTION/AVAILABILITY STATEMENT Approved for public release; distribution unlimited.				12b. DISTRIBUTION CODE	
13. ABSTRACT (Maximum 200 words) Two measurement techniques for investigating performance and life-limiting characteristics of ion engines are applied to a 10-cm T5 xenon thruster: (1) Thrust vector stability is evaluated with four double-wire Langmuir probes, aligned in the form of a cross, which are placed in the exhaust plume and are translated by a motorized positioning system to balance the currents collected along two orthogonal axes. The thrust vector position is thereby tracked with an angular resolution of < 0.01 deg and a response time of < 5 s. (2) A plume-sampling mass spectrometer has been developed for measuring the xenon charge state distribution and the flux of erosion products from the discharge chamber as a function of operating point. To demonstrate the capability for real-time erosion monitoring, plume spectra that reveal trace amounts of metal ions are presented. <div style="text-align: right;">DTIC QUALITY INSPECTED 8</div>					
14. SUBJECT TERMS Ion engine performance, plume measurements, thrust vector stability				15. NUMBER OF PAGES 15	
				16. PRICE CODE	
17. SECURITY CLASSIFICATION OF REPORT Unclassified	18. SECURITY CLASSIFICATION OF THIS PAGE Unclassified	19. SECURITY CLASSIFICATION OF ABSTRACT Unclassified		20. LIMITATION OF ABSTRACT	

Contents

I.	Introduction	1
II.	Beam-Centroid Tracking Instrument.....	2
III.	Plume-Sampling Mass Spectrometer.....	7
	References.....	10

Accession For	
NTIS CRA&I	<input checked="" type="checkbox"/>
DTIC TAB	<input type="checkbox"/>
Unannounced	<input type="checkbox"/>
Justification	
By	
Distribution/	
Availability Codes	
Dist	Avail and/or Special
A-1	

PLUME MEASUREMENTS WITH THE T5 XENON ION THRUSTER

James E. Pollard

*The Aerospace Corporation, Mechanics & Materials Technology Center,
P.O. Box 92957 - M5/754, Los Angeles, California 90009*

ABSTRACT

Two measurement techniques for investigating performance and life-limiting characteristics of ion engines are applied to a 10-cm T5 xenon thruster: (1) Thrust vector stability is evaluated with four double-wire Langmuir probes, aligned in the form of a cross, which are placed in the exhaust plume and are translated by a motorized positioning system to balance the currents collected along two orthogonal axes. The thrust vector position is thereby tracked with an angular resolution of $< 0.01^\circ$ and a response time of < 5 s. (2) A plume-sampling mass spectrometer has been developed for measuring the xenon charge state distribution and the flux of erosion products from the discharge chamber as a function of operating point. To demonstrate the capability for real-time erosion monitoring, plume spectra that reveal trace amounts of metal ions are presented.

I. INTRODUCTION

Spacecraft propulsion based on electrostatic acceleration of ions¹ has a long history of development in the United States,^{2,3} the United Kingdom,⁴ Germany,⁵ and Japan.⁶ The high exhaust velocity of ion thrusters (20-40 km/s) reduces the mass of propellant required for a given orbital maneuver, which can improve the payload capabilities, extend spacecraft maneuvering life, or reduce launch costs. These benefits have led to planned applications in geosynchronous stationkeeping on Japan's Engineering Test Satellite (ETS-6, 1994 launch)⁷ and on the European Space Agency's Advanced Relay and Technology Mission (ARTEMIS, 1996 or 1997 launch).⁸ However, ion thrusters have operating characteristics quite different from those of chemical propulsion systems, and incorporating them into a spacecraft design leads to challenges in regard to the mounting configuration, flight operations, and plume/spacecraft interactions.

Due to inherent manufacturing tolerances, there is a greater uncertainty in the position of the thrust vector (TV) for an ion engine than for a chemical thruster, which poses a difficulty in achieving the desired alignment relative to the spacecraft center-of-mass. Once on orbit, a long-term TV drift from grid erosion and a short-term drift during warm-up may lead to additional uncertainty. If left uncorrected, thrust misalignment generates disturbance torques and

can change the satellite's orbit in an undesired manner. Early consideration was given to TV control by electrostatic deflection of beamlets⁹ or by translating the ion accelerator grid as on NASA's Applications Technology Satellite (ATS-6, 1974 launch),¹⁰ but electromechanically gimbaling the entire thruster is now the most viable technology. Dual-axis gimbals were included with the mercury ion thrusters on NASA's Space Electric Rocket Test (SERT-II, 1970 launch), although the initial alignment proved to be entirely satisfactory without adjustment.¹¹ NASA later developed reduced-mass gimbal designs during the Ion Auxiliary Propulsion System (IAPS) and Solar Electric Propulsion System (SEPS) programs,² and a European gimbal is planned for use on the ARTEMIS mission.⁸

The ratio of output thrust to input electrical power is smaller for ion engines than for other electric propulsion devices such as resistojets, arcjets, and stationary plasma thrusters. As a result, the ion engine's operating life can be more important than the available mass of propellant in limiting the maneuvering life of a spacecraft. Because flight qualification may require a demonstrated operating time in excess of 10,000 hr (> 400 days), it is important to identify the most likely wear-out mechanism and to measure erosion rates as a function of operating parameters prior to initiating a full-duration life test. At operating points with high discharge voltage where there is significant production of multiply-charged species, internal erosion of the thruster tends to be the life-limiting factor.¹²⁻¹⁵ Multiple ionization also increases the ion production cost (watts per ampere) and requires that a correction factor be applied to thrust values calculated from the measured beam current. At operating points with reduced discharge voltage, the primary wear-out mechanism is erosion of the accelerator or decelerator grid caused by direct beam impingement or by charge-exchange ion impingement. Whether internal or external erosion is the overall life-limiter also depends on design features such as discharge volume, beam current density, magnetic field configuration (divergent or ring-cusp), materials of construction, and the use of sputter-resistant coatings.

To address some of the foregoing questions, this paper describes two new diagnostic methods, one for evaluating thrust vector stability and another for

measuring xenon charge states and the flux of eroding species in real time. They are illustrated by application to a 10-cm diameter ion thruster.

II. BEAM-CENTROID TRACKING INSTRUMENT

A. Apparatus description

Thrust measurement techniques for electric propulsion systems¹⁶ have been developed previously based on a spring restoring force, a pendulum, and a gas-bearing turntable, but these methods yield only the thrust magnitude along a single axis. In addition to thrust magnitude, the TV angular offset and stability must be measured to decide whether a given thruster will need on-orbit gimbaling, and to establish requirements for the gimbal angular range and slew rate. Experiments at Giessen University⁵ and at Culham Laboratory¹⁷ have used movable Faraday detectors (either single or multiplexed) to map the spatial distribution of ion flux in the exhaust plume, thereby monitoring the TV motion with a time-resolution of a few minutes. Flux maps are essential for understanding the transition of the plume from near-field to far-field behavior and for evaluating the beam divergence, but they contain more information than is usually necessary for evaluating TV offset and stability.

Our apparatus for locating the centroid of the ion beam¹⁸ achieves better time-resolution and is simpler to construct than a multiplexed Faraday detector. As shown in Fig. 1, four double-wire Langmuir probes (labeled North, South, East, West) are aligned in the form of a cross, and are suspended in the thruster plume 150-200 cm downstream of the exit plane. The detector is translated via a motorized positioning system to balance the currents collected along the North-South and East-West axes, thereby tracking the motion of the beam centroid in real time. The measurements reveal the absolute TV offset from the thruster centerline, the extent of TV drift during warm-up, and the dependence of TV position on thrust magnitude. This apparatus also records ion flux averaged over the radial extent of the plume, which is a useful diagnostic technique for routine verification of thruster performance. A beam-centroid tracking instrument could measure the TV offset during acceptance testing of ion thruster flight packages, which would afford an understanding of the unit-to-unit variation and would allow for shimming the engine mounts during integration with the spacecraft. The technique described here would also be useful for evaluating TV stability of stationary plasma thrusters, and it could find application in diagnosing broad-beam ion and plasma sources that are widely used for materials processing.¹⁹

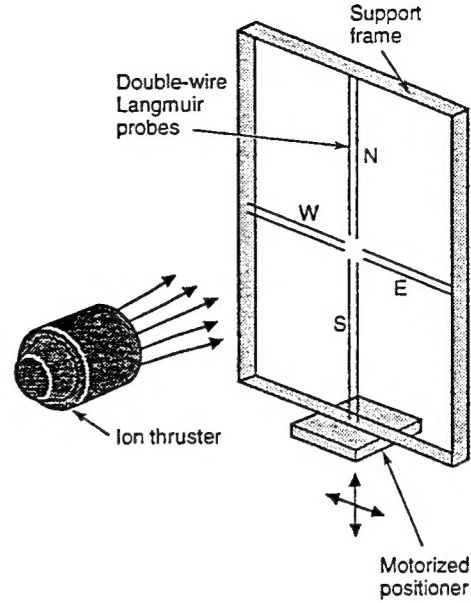


FIG. 1. Four double-wire Langmuir probes are suspended in the far-field plume of an ion thruster, and error signals are generated in proportion to the difference between the two probe currents along the North-South and East-West axes. The motorized positioner moves the assembly to null the error signals, thereby tracking the motion of the beam centroid.

A double-wire Langmuir probe²⁰ consists of two parallel conductors held in close proximity, which are electrically floating with respect to the surrounding plasma and which can be biased relative to each other for measurements of the current as a function of applied voltage. Theoretical considerations in the use of this device to measure ion flux and characteristic electron energy in the plume of a xenon ion thruster have been presented by deBoer.²¹ His analysis treats the case of a plasma in which the ions have a directed velocity much greater than their average thermal speed, and in which the electrons have a directed velocity much less than their average thermal speed. These conditions are satisfied by a thruster with 1-keV beam energy (40 km/s velocity), having a typical electron thermal speed ≥ 400 km/s and an ion thermal speed ≤ 4 km/s. Assuming that the electron distribution is Maxwellian with a temperature T_e , the probe current I as a function of applied voltage V is given by

$$I = n_i u_i e D L (1 + \eta) \tanh\left(\frac{e V}{2 k T_e}\right). \quad (1)$$

Here the ion density and directed velocity are n_i and u_i , the electronic charge and Boltzmann constant are e and k , the probe wire diameter and length are D and L , and the secondary electron yield is η . Probe current is zero in the absence of an applied voltage, but it

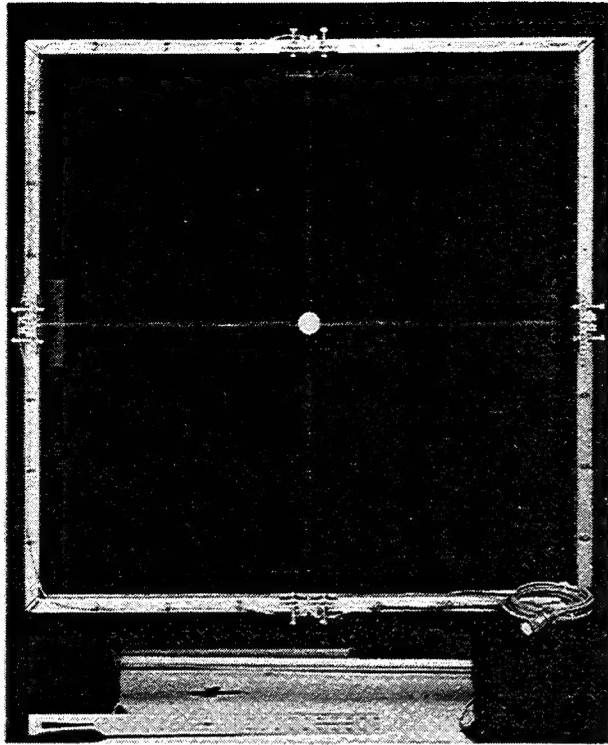


FIG. 2. Photo of the downstream side of the assembly showing probe wires, insulating hub, tensioners, support frame, and multipin connector.

approaches a saturation value I_{sat} with increasing voltage, namely

$$|I| \rightarrow I_{sat} \text{ for } |eV| \gg 2kT_e, \quad (2)$$

$$I_{sat} = n_i u_i e D L (1 + \eta).$$

According to the model, the two wires collect equal numbers of ions from the directed flow regardless of the voltage applied between them. At the asymptotic limit specified in Eq. (2), the negatively biased wire collects no electrons, and the positively biased wire collects a flux of electrons equal to the sum of the ion currents collected by both probe wires. This follows from the assumption that the probe assembly is electrically floating, and hence the net collected current must be zero under steady-state conditions. The foregoing analysis does not account for perturbation of the ion trajectories with increasing probe voltage, which causes the two probe wires to collect *different* numbers of ions and thereby show a gradually increasing probe current beyond the voltage at which the probe is "saturated" with respect to the electrons.

Probes for this experiment are constructed of various wire materials (0.40-mm diam Nichrome and 0.81-mm diam copper have been used successfully) and are supported by a 100-cm \times 100-cm square frame of welded aluminum channel (see Fig. 2). Each wire

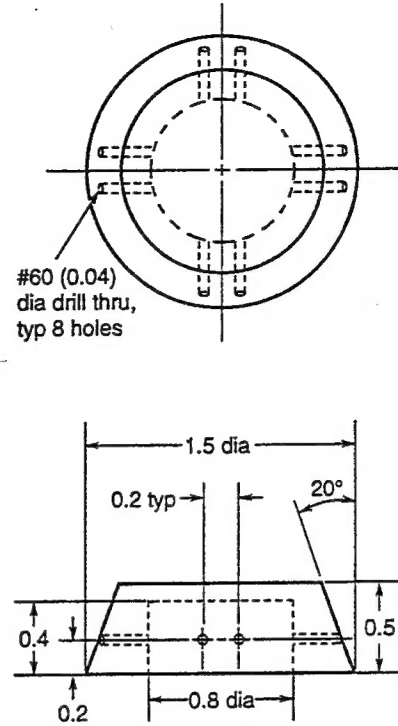


FIG. 3. Machine drawing of the boron nitride hub that holds the probe wires at the center of the assembly (dimensions in inches). Each of the eight wires is inserted through a radial hole and secured on the inside of the hub by bending the wire into a small kink or overhand knot. The upstream face of the hub is tapered by 20° to reduce the buildup of sputtered metal from the wires.

is secured at the supporting frame by a tensioning device that resembles the peg-and-nut mechanism of a violin. The tensioners are shielded from direct beam impingement to avoid spurious currents that would introduce an error in the absolute position of the beam centroid. An insulating hub made of boron nitride (see Fig. 3) holds the probes at the center of the assembly and establishes a wire spacing of 5 mm. During ion bombardment, sputtered metal from the wires is deposited on the insulating hub and eventually can cause an electrical short between the wires. To alleviate this problem the hub is tapered in the upstream direction so that most of the deposits are removed by exposure to the incident ion beam. Each probe has an effective length of $L = 42$ cm after accounting for the tensioner-shield and insulating hub. When placed 200 cm downstream of the ion accelerator grid, the assembly samples the beam within a 12° half-angle from thruster centerline. The accelerator grid normal axis (i.e., centerline) is located by holding a 25-mm diam mirror against the grid center and observing the back-reflection from 4-5 meters away. Repeated independent trials show that the experimental error in locating this axis is $\pm 0.3^\circ$, which is also the estimated uncertainty in the absolute

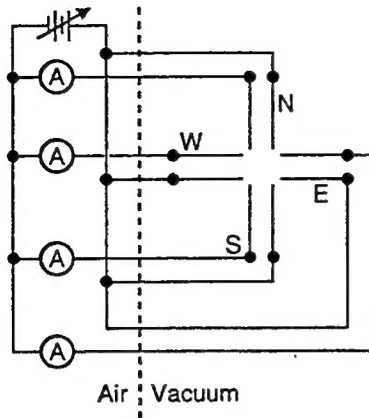


FIG. 4. Electrical schematic showing the four individual probe wires connected to digital ammeters, and the four common probe wires connected to the dc power supply. Positive probe voltage is defined as the four common wires being at a positive potential relative to the four individual wires. An alternative configuration using four separate dc power supplies with no common probe wires has also been tested.

TV position. This error could be reduced by constructing a custom alignment fixture rather than using a hand-held mirror. A three-axis motorized positioning system with a resolution of 10 steps/ μm (Compumotor 4000) is used for translation of the probe assembly; its coordinate origin is established by aligning the probe axes so as to intersect thruster centerline.

The electrical arrangement uses four digital ammeters (Fluke 45, full scale of 9.9999 mA) and one variable bias supply (HP 6216B) with four of the eight probe wires connected in common (see Fig. 4). Probe signals are carried by shielded multi-conductor cables that are routed along the back side of the support frame and from there to a vacuum feedthrough. A laboratory computer reads the four ammeters and commands the positioning system to move a vertical distance d_v that is proportional to the North/South error signal and to move a horizontal distance d_h proportional to the East/West error signal, thereby balancing the currents and tracking the motion of the centroid in real time. Distances are calculated using

$$d_v = G \times (I_N - I_S) / (I_N + I_S), \quad (3)$$

$$d_h = G \times (I_E - I_W) / (I_E + I_W), \quad (4)$$

where I_N, I_S, I_E, I_W are the four probe currents, and a feedback gain of $G = 150 \text{ mm}$ serves to balance the currents rapidly with minimal overshoot. The computer automatically halts the tracking cycles if the current drops below a preset value (i.e., the ion beam turns off) or if the current goes above a preset value (i.e., an electrical short develops between the probe wires). For a typical reading of $140.0 \mu\text{A}$, a change in

TABLE I. Operating conditions for the T5 ion engine at a nominal thrust of 25 mN. An electrical schematic of the thruster power supply appears in Ref. 4. Xenon flow rates are 0.74 mg/s (main discharge), 0.10 mg/s (main hollow cathode), and 0.033 mg/s (neutralizer hollow cathode). Facility pressure as measured by a corrected ionization gauge is 2.7×10^{-6} torr.

Power Supply	Voltage (V)	Current (mA)
Ion beam	1100	453
Main discharge	41.6	3010
Electromagnet	12.7	172
Accelerator grid	-350	2.10
Main cathode	12.6	1000
Neutralizer cathode	19.5	720

the least significant ammeter digit ($\pm 0.1 \mu\text{A}$) causes the positioning system to move by $\pm 0.06 \text{ mm}$, which amounts to a TV angular motion of $\pm 0.002^\circ$. Each cycle of reading the four currents and moving the probe assembly takes 2.4 seconds on average.

B. Results and discussion

The test article is a divergent-field xenon ion thruster (10-cm diameter, two grid, engineering-model T5 Mk3) manufactured by the UK Defence Research Agency,⁴ and it performs as listed in Table I when operated in a vacuum facility at Aerospace Corp. A distinctive feature of the T5 thruster is that the screen grid and accelerator grid are dished inward to prevent a short circuit from occurring due to differential thermal expansion. The resulting convergent trajectories of the ion beamlets produce a beam waist 10-15 cm downstream of the accelerator grid. Background pressure during the test is maintained in the low 10^{-6} torr range by two re-entrant closed-cycle cryopumps (CVI TM1200) with a combined pumping speed of 7×10^4 liter/s for xenon. The beam dump consists of a water-cooled aluminum plate coated with graphite (Aquadag-E) that is located 50-70 cm downstream of the beam-centroid instrument.

Langmuir probe current-voltage characteristics are shown in Fig. 5 for operation at a nominal thrust of 19 mN. A positive probe voltage (e.g., +5 V) means that the four *common* wires are positive with respect to the four *individual* wires that lead to the ammeters; in this case the individual wires collect only ions at saturation, while the common wires collect both electrons and ions. The traces in Fig. 5 are measured when the probe assembly is positioned so as to equalize the currents at a voltage of +5 V. A

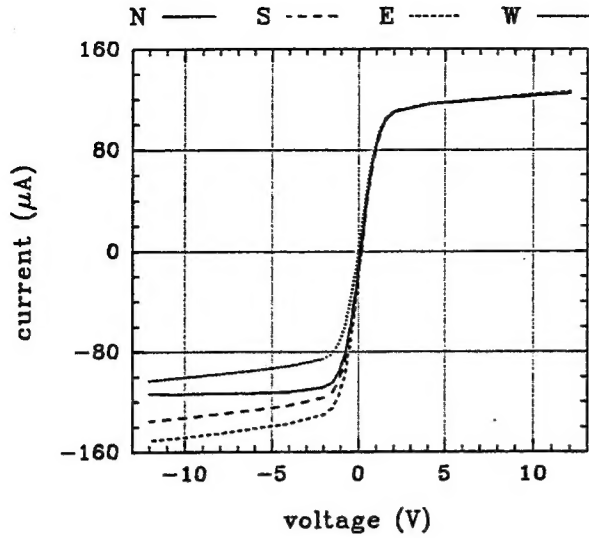


FIG. 5. Langmuir probe current-voltage characteristics for the beam-centroid instrument when the thruster is operated at 19 mN. The probe assembly is 201 cm from the ion accelerator grid and is positioned to balance the currents at a probe voltage of +5 V. The discrepancy between the four currents at negative voltage is discussed in the text.

discrepancy is noted between the four currents when the voltage is negative, but the average of the four currents at negative voltage matches the average at the corresponding positive voltage to within 0.7%. The most likely explanation for the behavior at negative voltage is that different numbers of electrons are collected by the individual wires (e.g., more go to the East than to the West), possibly due to gradients in the electron temperature. For positive probe voltages the instrument is relatively immune to this effect, because at saturation the individual wires do not collect any electrons, and hence the ammeters respond only to ion currents. An alternative configuration has been tested using four separate power supplies with no wires connected in common. In this case the four probes show identical, symmetric current-voltage characteristics, and the measured centroid position is the same as when the standard configuration is operated at positive common probe voltage. Nearly all of the beam centroid data that we have recorded are with the standard configuration at +5 V.

Figure 6 shows the average of the four probe currents as a function of voltage. Between -3 V and +3 V the data are well-represented by the hyperbolic tangent function in Eq. (1), but outside this range the magnitude of the current continues to increase linearly rather than reaching a saturation value. The probable cause is perturbation of ion trajectories as mentioned in Section II.A, but there may also be a contribution from increasing secondary electron yield. A least-squares fit to the data in Fig. 6 gives $I_{sat} = 111.5 \mu\text{A}$

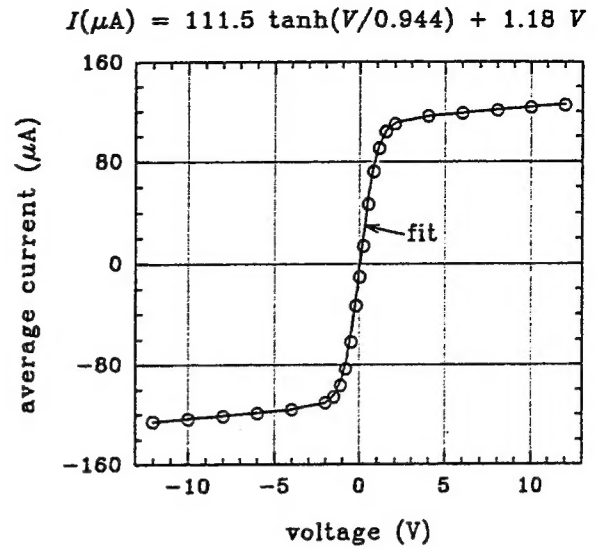


FIG. 6. Current-voltage characteristic averaged over the four probes at 19 mN nominal thrust. Open circles are the measurements, and the solid line is a least-squares fit using Eq. (1) plus a linear term to represent post-saturation behavior (see Sec. II.A). The average of the four currents at negative voltage matches the average at the corresponding positive voltage to within 0.7%.

and $kT_e = 0.47 \text{ eV}$. The ion flux averaged over the radial extent of the plume at 201 cm from the accelerator grid is then

$$n_i u_i e R^2 = \frac{I_{sat} R^2}{D L (1 + \eta)} \quad (5)$$

$$= \frac{(111.5 \mu\text{A})(201 \text{ cm} - 15 \text{ cm})^2}{(0.040 \text{ cm})(42 \text{ cm})(1.019)} = 2.3 \text{ A sr}^{-1}.$$

Here the ion flux per steradian is calculated with respect to a beam waist located 15 cm downstream of the accelerator grid, and the secondary electron yield is that of 1-kV xenon ions on tungsten.²¹ For comparison with Eq. (5), an independent measurement in our facility using smaller Langmuir probes gives a centerline ion flux of 2.0-2.5 A sr⁻¹ at 35-60 cm from the accelerator grid (nominal thrust of 18 mN).²¹

Relative positional accuracy of the beam-centroid instrument is checked using a separate translation system to move the thruster vertically in steps of 1.02 cm while observing the motion of the probe assembly (see Fig. 7). The vertical response matches the thruster motion to within $\pm 1\%$, while the horizontal response (i.e., cross coupling) is 1-2% of the nominally vertical thruster motion. The settling time at each vertical step corresponds to a maximum instrument slew rate of 2.4 cm per minute and a maximum centroid motion of 0.7° per minute.

A possible source of error in the TV offset is spurious current collected at the edges of the ion beam

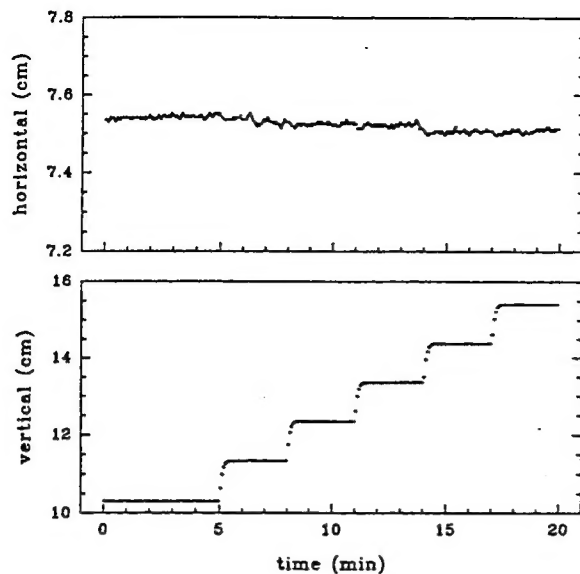


FIG. 7. Instrument response as the thruster is translated in 1.02-cm steps by a vertical motion system. Beam-centroid vertical motion matches the thruster motion to within $\pm 1\%$. Scale for the horizontal axis is magnified by a factor of 10 to show cross-coupling.

by the probe-wire tensioners (despite the effort to shield them). This error is shown to be minimal by monitoring the apparent centroid position while changing the distance between the thruster and the probe assembly: the centroid moves by less than 0.05° when the distance is varied from 155 cm to 201 cm. Possible errors due to ions scattered from the beam dump are also shown to be negligible by this observation. Because the probe wires collect only a small fraction of the total ion flux, the thrust vector measurement accuracy would be degraded if the plume deviated strongly from azimuthal symmetry. Tests on a two-grid T5 thruster at Culham Laboratory using a movable Faraday detector showed that the plume is azimuthally symmetric to within 2-3%,¹⁷ which justifies the assumption underlying our beam-centroid experiment.

TV behavior for a cold start at 25 mN is given in Fig. 8, showing a warm-up drift of 0.3° in 40 minutes, and steady-state offsets of -1.2° horizontal and -1.2° vertical, relative to thruster centerline. (Referring to Fig. 1, the negative horizontal and vertical directions are identified with the West and South axes, respectively.) Prior to a recent realignment of the thruster grid assembly, the offset at 25 mN was -1.3° horizontal and -3.3° vertical, which suggests that TV position is substantially affected by the grid alignment procedure. Independent verification of the absolute offset is obtained from a limited set of beam profile scans made in our facility using a Faraday detector, which agrees with the beam centroid results to within the combined uncertainties ($\pm 0.5^\circ$). Tests at Culham

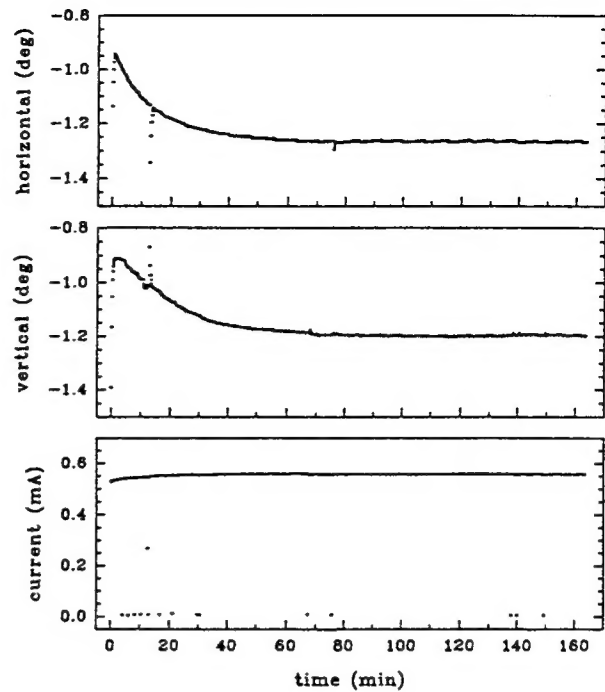


FIG. 8. Thrust vector drift following a cold start at a nominal thrust of 25 mN, with horizontal and vertical deflection given in degrees relative to thruster centerline. The currents are unbalanced for the first five data points while the instrument converges on the centroid position. The lower trace is the summed probe current, which goes to zero several times during this data set when the thruster experiences a momentary grid short followed by a restart.

Laboratory with a movable Faraday detector also found significant steady-state offsets (0.5° horizontal, 2.4° vertical).¹⁷ The UK-10 flight unit will use a three-grid design exhibiting somewhat different thrust vector drift than the two-grid version tested here,¹⁷ and we are currently setting up for centroid measurements on a three-grid engine.

When the warm-up drift is fairly small, it may be possible to save spacecraft cost and mass by eliminating the need for thruster gimbals, but this would require testing to establish how much the thrust vector has moved after accumulating thousands of operating hours. Warm-up drift for the two-grid thruster tested here (0.3°) is small enough to be compensated in most applications by the spacecraft attitude control system or by thruster gimbaling, but the absolute offset from centerline (1.2°) indicates that shimming of the engine mount will likely be needed during integration with the spacecraft. The current design for the ARTEMIS gimbal allows a maximum canting angle of 5° , and the intent is to launch with the thruster secured in the nominal center position to allow for stationkeeping in the event of a gimbal failure.⁸

The dependence of TV position on thrust level is presented in Fig. 9, showing motions of about 0.2°

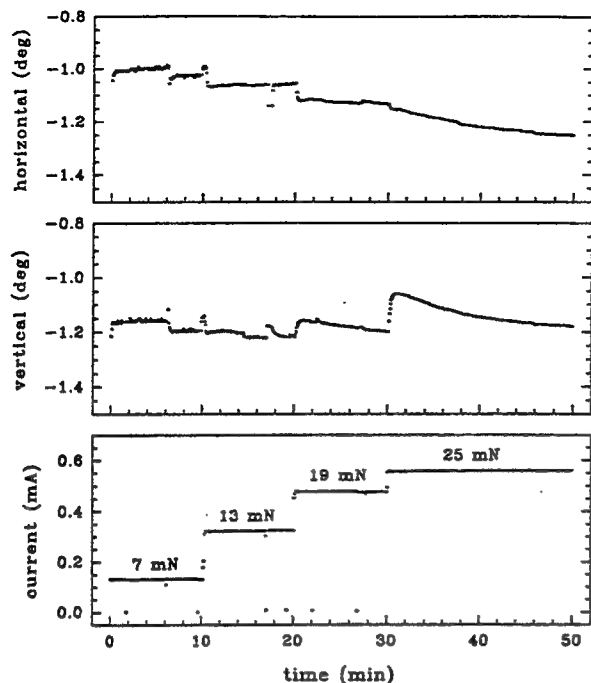


FIG. 9. Thrust vector behavior with a fully warmed up engine when the beam current is varied to give nominal thrusts of 7, 13, 19, and 25 mN. The lower trace is the summed probe current, which goes to zero several times during this data set when the thruster experiences a momentary grid short followed by a restart.

over the range of 7 mN to 25 mN. Granularity is evident in the 7-mN data due to the 0.1- μ A resolution of the ammeters. Following a change in thrust, the short-term TV displacement is faster than the instrument response, and the longer-term displacement has a time constant of 10-20 minutes. A valuable adjunct to the centroid measurements will be to correlate the TV motion with the thruster grid deformations that we have observed recently using telemicroscopic video cameras.²² The screen and accelerator grids have different time constants for thermal expansion, and the telemicroscope shows how the gap between the grids varies as a function of discharge power. Differential thermal expansion of the grids is implicated as the primary cause for the observed TV motions.

III. PLUME-SAMPLING MASS SPECTROMETER

A. Apparatus description

Measurements of charge state distributions in ion engine plumes have been used to derive thrust correction factors and to identify operating points where internal erosion is likely to be at a minimum. One technique for accomplishing this is the $E \times B$ analyzer, which separates ions according to their mass-to-charge ratio and can be assembled as a compact probe suitable for multipoint sampling within

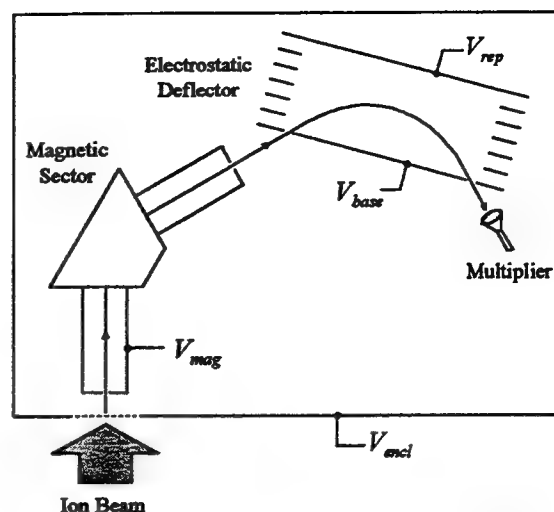


FIG. 10. Ions from the thruster plume are selected according to their mass-to-charge ratio by a 60° magnetic sector and are filtered by a parallel-plate electrostatic deflector to enhance resolution. The ion current is amplified by a ceramic electron multiplier and recorded by a digital picoammeter. The aluminum enclosure is held at a few volts negative with respect to the floating potential of the plasma in order to suppress the background due to electrons.

the plume.^{13, 23-26} A second proven technique consists of a pulsed ion beam time-of-flight analyzer, again configured as a probe with the capability for spatially resolved studies.^{17, 27} The mass-to-charge resolving power of $E \times B$ and time-of-flight analyzers is adequate for separating propellant ions into their various charge states, but these devices have not thus far detected trace amounts of thruster erosion products. Instead, the assessment of erosion rates has relied on deposition monitors such as witness plates, solar cells, and quartz crystal microbalances, or on inspecting the thruster using photographic and mass-depletion measurements, but these methods do not allow real-time identification of eroding species. Optical techniques using emission spectroscopy and laser-induced fluorescence are viable real-time diagnostics for the neutral molybdenum efflux produced by impingement of charge-exchange ions on the accelerator grid.^{28, 29}

Our experiment uses a magnetic sector mass spectrometer designed to have higher mass-to-charge resolution than existing $E \times B$ and time-of-flight analyzers and to achieve sufficient selectivity to discriminate between the majority and trace species in the plume. Figure 10 shows the mass spectrometer in its current configuration with a 60° magnetic sector³⁰ followed by a parallel-plate electrostatic deflector.³¹ The instrument can sample the plume at various distances and angles using a motorized positioning system, but so far we have only collected data along the thruster centerline. Ions generated within the

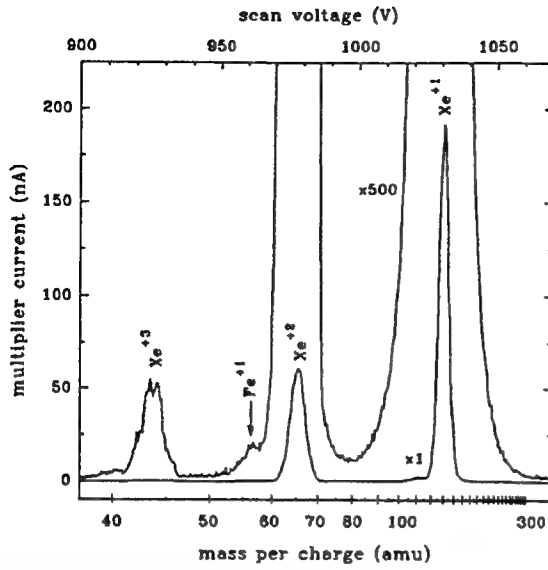


FIG. 11. Mass spectrum measured along the centerline of the plume at a nominal thrust of 18 mN. The discharge voltage and current are 35.9 V and 3.01 A, the magnet current is 100 mA, and the beam voltage and current are 1100 V and 332 mA. The results have not been corrected for the relative sensitivity of the spectrometer as a function of mass and charge state.

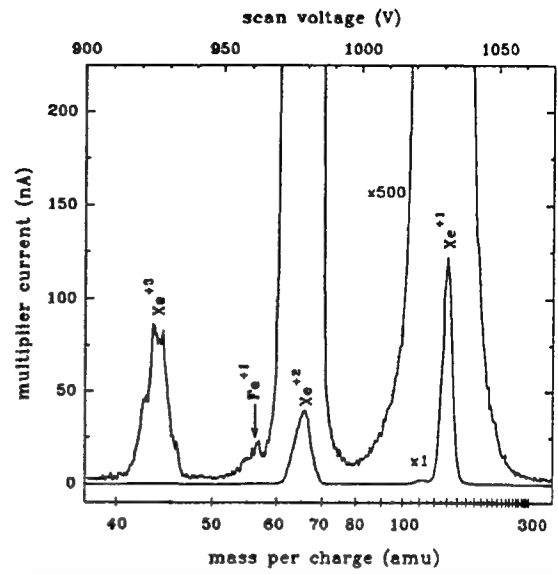


FIG. 12. Mass spectrum measured along the centerline of the plume at a nominal thrust of 22 mN. The discharge voltage and current are 38.3 V and 3.01 A, the magnet current is 140 mA, and the beam voltage and current are 1100 V and 405 mA. The results have not been corrected for the relative sensitivity of the spectrometer as a function of mass and charge state.

main discharge are accelerated on leaving the thruster to a nominal beam energy of

$$E_{beam} = n e V_{screen}, \quad (6)$$

where n is the charge state of the ion, and the screen grid potential relative to the vacuum chamber ground is $V_{screen} = +1100$ V. After travelling downstream for 180 cm, the ions pass through a stainless steel mesh into the detector enclosure. The enclosure is held negative with respect to the plasma floating-potential to prevent electrons from entering (e.g. $V_{encl} = +6$ V, $V_{float} \approx +8$ V). The kinetic energy of ions transmitted by the magnetic sector is

$$E_{mag} = n e (V_{screen} - V_{mag}) = \frac{(n e B R)^2}{2m}, \quad (7)$$

where m is the ion mass, B is the magnetic induction (0.235 tesla), R is the radius of curvature (51 mm), and V_{mag} is the potential of the magnetic sector beam tube. Solving for the mass-to-charge ratio in terms of the apparatus parameters, we have

$$\frac{m}{n e} = \frac{(B R)^2}{2 (V_{screen} - V_{mag})}. \quad (8)$$

The use of a permanent magnet helps to keep the design simple and relatively compact, and it means that V_{mag} (rather than B) is swept to record a mass spectrum. Equations (7) and (8) apply to ions that are produced within the discharge chamber and accelerated to the nominal beam energy, but they do not apply to lower energy ions (e.g., charge exchange)

that are produced downstream and are not detected in this experiment.

The magnetic sector with 50-100 μm slits has, by itself, sufficient resolution to separate the xenon charge states, but to search for erosion products an energy selector must be included in series with the mass-dispersing stage. This is because the broadened energy distribution of the ions ($\Delta E_{beam} \approx 12$ eV full-width at half maximum) leads to tailing of the xenon mass peaks and makes it difficult to detect trace species against the intense, sloping background. Figure 10 shows the parallel plate energy analyzer located downstream of the magnetic sector, with the entrance slit, exit slit, and base plate at a potential V_{base} , and the repeller plate at a potential close to that of the thruster screen grid ($V_{rep} \approx V_{screen}$). The potentials V_{base} and V_{rep} are held constant while V_{mag} is varied to scan through the mass spectrum. In the present arrangement the energy analyzer launch-angle is 45° , the distance between the entrance and exit slits (152 mm) is twice the distance between the base plate and the repeller, and consequently the analyzer pass energy has the simple form³¹

$$E_{pass} = n e (V_{rep} - V_{base}). \quad (9)$$

Here E_{pass} is the kinetic energy of an ion at the moment it passes through the analyzer exit slit; the kinetic energy that this ion had when it was in the plume (i.e., the energy being analyzed) is determined only by the repeller potential, namely $E_{beam} = n e V_{rep}$.

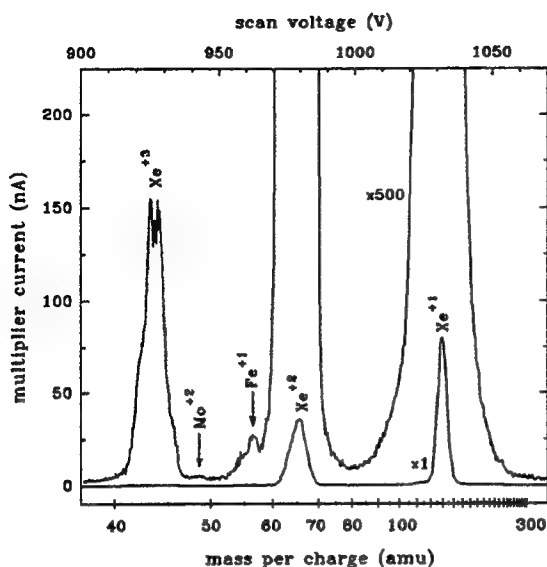


FIG. 13. Mass spectrum measured along the centerline of the plume at a nominal thrust of 26 mN. The discharge voltage and current are 41.3 V and 3.01 A, the magnet current is 180 mA, and the beam voltage and current are 1100 V and 472 mA. The results have not been corrected for the relative sensitivity of the spectrometer as a function of mass and charge state.

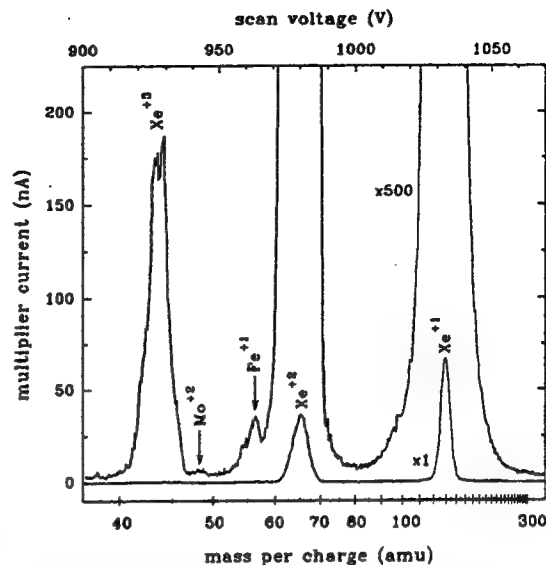


FIG. 14. Mass spectrum measured along the centerline of the plume at a nominal thrust of 28 mN. The discharge voltage and current are 43.1 V and 3.01 A, the magnet current is 200 mA, and the beam voltage and current are 1100 V and 504 mA. The results have not been corrected for the relative sensitivity of the spectrometer as a function of mass and charge state.

For a pass energy of $E_{\text{pass}} = 400$ eV and a slit width of 1.5 mm, the theoretical energy bandpass is 2 eV, and the mass peaks have an observed full-width at half maximum of $\Delta V_{\text{mag}} = 5$ V, as compared with the mass spectra recorded using the magnetic sector alone, which have peak widths of $\Delta V_{\text{mag}} = 12$ V.

B. Results and discussion

Mass spectra of the plume are shown in Figs. 11-14 with the main discharge current held constant at 3.01 A, the magnet current set to 100, 140, 180, and 200 mA to vary the operating point, and the other parameters as listed in the figure captions or in Table I. The three largest features in these spectra are due to Xe^{+1} , Xe^{+2} , and Xe^{+3} , and their relative intensities change over a substantial range in Figs. 11-14. The overall signal level drops as thrust increases, mainly because the plume energy distribution broadens (hence the analyzer bandpass transmits a smaller fraction of the ions), and to a smaller extent because the plume divergence increases (hence the detector angular acceptance transmits a smaller fraction of the ions). Ramping up the magnet current increases the discharge voltage from 36 V to 43 V, which causes the ion populations to shift toward Xe^{+2} and Xe^{+3} . Extending the mass spectrum to lower scan voltage shows that Xe^{+4} is not produced in measurable amounts at any of the operating points tested here.

We would like to obtain quantitative information about xenon charge state distributions from these data sets, but this is impractical because the relative

sensitivity of the spectrometer as a function of mass and charge state is observed to depend on the repeller potential of the electrostatic deflector. In principle, mass spectra could be recorded at many repeller potentials to determine the integrated intensities, but a more efficient approach may be to use the magnetic sector alone since it has sufficient resolution to separate the xenon charge states. Another difficulty with the present setup is that exposure to the ion beam degrades the retarding-field electrodes at the magnetic sector entrance, which causes a gradual loss of sensitivity and resolution. This is a possible cause of a small peak with varying intensity at about 110 amu (see Figs. 11, 12), for which no plausible ion can be assigned and which is likely an artifact. We are continuing to evaluate modified electrode and aperture designs that may be less susceptible to this problem.

The amplified traces in Figs. 11-14 reveal a peak at 56 amu that is identified as singly charged iron Fe^{+1} , and a weaker feature centered at 48 amu that is identified as doubly charged molybdenum Mo^{+2} (expected isotopic distribution is 46-50 amu). Both of these signals have a dependence on operating conditions that is consistent with an erosion product, namely they increase appreciably relative to Xe^{+1} and Xe^{+2} as the discharge voltage increases. There are no common residual gases that could lead to signals of the observed magnitude at 48 and 56 amu, although we do see residual gas peaks at 12-18 amu and at 28 amu when the scan is extended to the lower mass range. One would reasonably expect Fe^{+1} to be

produced by internal erosion of the T5 thruster, because the discharge chamber and anode are made of stainless steel ($\approx 70\%$ Fe), and the pole pieces and back plate are made of soft iron (initially plated with nickel). For Mo^{+2} ions to be detected in this experiment, they must have a beam energy of 2×1100 eV, which indicates that they originate from sputtering of the screen grid rather than the accelerator grid.

Following a 500-hr test at Culham Laboratory with discharge voltages of 39-52 V, significant erosion from the discharge chamber, back plate, and pole pieces was observed, along with smaller mass losses from the anode and screen grid.¹² Sputtered deposits found within the thruster following the Culham test were mainly iron, nickel, and molybdenum. Signals from Ni^{+1} (at 58 and 60 amu) and from Mo^{+1} (at 92-100 amu) are not discernable in our spectra, but they would be more difficult to detect than Fe^{+1} and Mo^{+2} because of the sloping background from the nearby Xe^{+2} and Xe^{+1} peaks. Similarly, the expected erosion products from the cathode (barium, tungsten) and the baffle disk (tantalum) are likely to be lost in the high-mass tail of Xe^{+1} with the present configuration of the apparatus.

As an order-of-magnitude check on the plausibility of the observed Fe^{+1} intensity, we note that it is smaller than the Xe^{+1} signal by about a factor of 2000, which implies the Fe^{+1} current is $\approx 1 \times 10^{15} \text{ s}^{-1}$ or, equivalently, 0.2 g per 500 hr. This is not inconsistent with the observed mass loss from stainless steel and iron components in the Culham test, which was in the range of 0.1-3.5 g per 500 hr depending on the discharge voltage.

We are planning additional experiments to confirm the identification of the metal ion signals and to establish the transmission of the spectrometer as a function of mass-to-charge ratio. The goal is to obtain quantitative erosion data that can be compared with mass loss rates and charge-state distributions measured elsewhere. The expected benefit of this work is an ability to predict thruster lifetime as a function of operating point. Another planned experiment will use the electrostatic deflector for directly measuring the energy spread of the beam to improve our ability to model the discharge behavior.

ACKNOWLEDGEMENTS

The author had the benefit of discussions with P.C.T. deBoer, S.W. Janson, P.M. Latham, L.K. Johnson, R.P. Welle, and M.W. Crofton. This work is sponsored by the US Air Force Space and Missile Systems Center, Division of Advanced Plans under contract number F04701-88-C-0089, with funds

provided by the Foreign Comparative Test Program of the Secretary of the Air Force. Department of Defense review of this material does not imply endorsement of factual accuracy or opinion.

REFERENCES

1. G.P. Sutton, *Rocket Propulsion Elements*, 6th ed. (Wiley, New York, 1992), pp. 580-590.
2. V.K. Rawlin, M.J. Patterson, and R.P. Gruber, "Xenon ion propulsion for orbit transfer," Paper AIAA-90-2527, 21st International Electric Propulsion Conference, 18-20 July 1990, Orlando, Florida.
3. J.R. Beattie, J.N. Matossian, and R.R. Robson, "Status of xenon ion propulsion technology," *J. Propulsion and Power*, **6**, 145 (1990).
4. D.G. Fearn, A.R. Martin, and P. Smith, "Ion propulsion research and development in the UK," *J. Brit. Interplan. Soc.* **43**, 431 (1990).
5. K.H. Groh and H.W. Loeb, "Radio-frequency ion sources for space propulsion," *Rev. Sci. Instrum.* **63**, 2513 (1992).
6. Y. Arakawa, "Review of electric propulsion activities in Japan," Paper IEPC-93-005, 23rd International Electric Propulsion Conference, 13-16 Sept 1993, Seattle, Washington.
7. S. Shimada, et al. "Development of ion engine system for ETS-6," Paper IEPC-93-009, 23rd International Electric Propulsion Conference, 13-16 Sept 1993, Seattle, Washington.
8. H. Bassner, et al. "Ion propulsion: A key enabler on ESA's DRTM programme," Paper IEPC-93-059, 23rd International Electric Propulsion Conference, 13-16 Sept 1993, Seattle, Washington.
9. H.J. King and D.E. Schnelker, "Ion thruster systems with thrust vector deflection," *J. Spacecraft and Rockets*, **8**, 552 (1971).
10. K.E. Clark, "Survey of electric propulsion capability," *J. Spacecraft and Rockets*, **12**, 641 (1975).
11. W.R. Kerslake and L.R. Ignaczak, "Development and flight history of the SERT-II spacecraft," *J. Spacecraft and Rockets*, **30**, 258 (1993).
12. D.G. Fearn, "Ion thruster lifetime limitations imposed by sputtering processes," Paper IEPC-93-177, 23rd International Electric Propulsion Conference, 13-16 Sept 1993, Seattle, Washington.
13. M.J. Patterson, "Performance characteristics of ring-cusp thrusters with xenon propellant," Paper AIAA-86-1392, 22nd Joint Propulsion Conference, 16-18 June 1986, Huntsville, Alabama.
14. M.J. Patterson, "Low- I_{sp} derated ion thruster operation," Paper AIAA-92-3203, 28th Joint Propulsion Conference, 6-8 July 1992, Nashville, Tennessee.
15. S. Shimada, et al. "Ion thruster endurance test using development model thruster for ETS-6," Paper IEPC-93-169, 23rd International Electric Propulsion Conference, 13-16 Sept 1993, Seattle, Washington.

16. H. Murakami, et al. "Thrust measurement of an ion engine system," *J. Spacecraft and Rockets*, **21**, 96 (1984); W.E. Morren, et al. "Performance and endurance tests of a laboratory model multipropellant resistojet," *J. Propulsion and Power*, **6**, 18 (1990); T.W. Haag, "Thrust stand for high-power electric propulsion devices," *Rev. Sci. Instrum.* **62**, 1186 (1991); A. Sasoh and Y. Arakawa, "A high-resolution thrust stand for ground tests of low-thrust space propulsion devices," *Rev. Sci. Instrum.* **64**, 719 (1993).
17. S.D. Watson, et al. "500 hour tests of the T5 ion thruster with dual and triple grid extraction systems," Paper IEPC-93-170, 23rd International Electric Propulsion Conference, 13-16 Sept 1993, Seattle, Washington.
18. J.E. Pollard, "Beam-centroid tracking instrument for ion thrusters," *Rev. Sci. Instrum.* (submitted).
19. See for example, H.R. Kaufman and R.S. Robinson, "Ion source design for industrial applications," *AIAA Journal*, **20**, 745 (1982); and B.H. Wolf, editor, Proceedings of the 4th International Conference on Ion Sources, *Rev. Sci. Instrum.*, Vol. 63, No. 4, Part II (1992).
20. N. Hershkowitz, "How Langmuir probes work," in Plasma Diagnostics, edited by O. Auciello and D.L. Flamm (Academic, San Diego, 1989), Vol. 1, pp. 176-178.
21. P.C.T. deBoer, "Electric probe measurements in the plume of the UK-10 ion thruster," Paper IEPC-93-236, 23rd International Electric Propulsion Conference, 13-16 Sept 1993, Seattle, Washington.
22. M.W. Crofton, "Test and evaluation of the T5 (UK-10) ion engine: program status," Paper AIAA-94-2847, 30th Joint Propulsion Conference, 27-29 June 1994, Indianapolis, Indiana.
23. R.P. Vahrenkamp, "Measurement of double charged ions in the beam of a 30-cm mercury bombardment thruster," Paper AIAA-73-1057, 10th Electric Propulsion Conference, 31 Oct - 2 Nov 1973, Lake Tahoe, Nevada.
24. J.S. Sovey, "Improved ion containment using a ring-cusp ion thruster," *J. Spacecraft and Rockets*, **21**, 488 (1984).
25. Y.-Z. Kuang, G.-Q. Qing, and S.-T. Yang, "ExB momentum analyzer for broad-beam ion sources," Paper AIAA-87-1081, 19th International Electric Propulsion Conference, 11-13 May 1987, Colorado Springs, Colorado.
26. H. Takegahara, et al. "Beam characteristics evaluation of ETS-6 xenon ion thruster," Paper IEPC-93-235, 23rd International Electric Propulsion Conference, 13-16 Sept 1993, Seattle, Washington.
27. M.S. Harvey, et al. "The advanced propulsion space test facilities at AEA Technology, Culham Laboratory," Paper IEPC-91-153, 22nd International Electric Propulsion Conference, 14-17 Oct 1991, Viareggio, Italy.
28. B.A. Rock, M.A. Manteniaks, and M.L. Parsons, "Rapid evaluation of ion thruster lifetime using optical emission spectroscopy," Paper AIAA-85-2011, 18th International Electric Propulsion Conference, 30 Sept - 2 Oct 1985, Alexandria, Virginia.
29. C.J. Gaeta, et al. "Erosion rate diagnostics in ion thrusters using laser-induced fluorescence," *J. Propulsion and Power*, **9**, 369 (1993).
30. J.B. Farmer, "Types of mass spectrometers," in Mass Spectrometry, edited by C.A. McDowell (McGraw-Hill, New York, 1963), p. 7.
31. J. Berkowitz, Photoabsorption, Photoionization, and Photoelectron Spectroscopy (Academic Press, New York, 1979), p. 443.

TECHNOLOGY OPERATIONS

The Aerospace Corporation functions as an "architect-engineer" for national security programs, specializing in advanced military space systems. The Corporation's Technology Operations supports the effective and timely development and operation of national security systems through scientific research and the application of advanced technology. Vital to the success of the Corporation is the technical staff's wide-ranging expertise and its ability to stay abreast of new technological developments and program support issues associated with rapidly evolving space systems. Contributing capabilities are provided by these individual Technology Centers:

Electronics Technology Center: Microelectronics, solid-state device physics, VLSI reliability, compound semiconductors, radiation hardening, data storage technologies, infrared detector devices and testing; electro-optics, quantum electronics, solid-state lasers, optical propagation and communications; cw and pulsed chemical laser development, optical resonators, beam control, atmospheric propagation, and laser effects and countermeasures; atomic frequency standards, applied laser spectroscopy, laser chemistry, laser optoelectronics, phase conjugation and coherent imaging, solar cell physics, battery electrochemistry, battery testing and evaluation.

Mechanics and Materials Technology Center: Evaluation and characterization of new materials: metals, alloys, ceramics, polymers and their composites, and new forms of carbon; development and analysis of thin films and deposition techniques; nondestructive evaluation, component failure analysis and reliability; fracture mechanics and stress corrosion; development and evaluation of hardened components; analysis and evaluation of materials at cryogenic and elevated temperatures; launch vehicle and reentry fluid mechanics, heat transfer and flight dynamics; chemical and electric propulsion; spacecraft structural mechanics, spacecraft survivability and vulnerability assessment; contamination, thermal and structural control; high temperature thermomechanics, gas kinetics and radiation; lubrication and surface phenomena.

Space and Environment Technology Center: Magnetospheric, auroral and cosmic ray physics, wave-particle interactions, magnetospheric plasma waves; atmospheric and ionospheric physics, density and composition of the upper atmosphere, remote sensing using atmospheric radiation; solar physics, infrared astronomy, infrared signature analysis; effects of solar activity, magnetic storms and nuclear explosions on the earth's atmosphere, ionosphere and magnetosphere; effects of electromagnetic and particulate radiations on space systems; space instrumentation; propellant chemistry, chemical dynamics, environmental chemistry, trace detection; atmospheric chemical reactions, atmospheric optics, light scattering, state-specific chemical reactions and radiative signatures of missile plumes, and sensor out-of-field-of-view rejection.



2350 E. El Segundo Boulevard
El Segundo, California 90245-4691
U.S.A.